



HAL
open science

Analogues of interplanetary dust particles to interpret the zodiacal light polarization

Edith Hadamcik, Jérémie Lasue, Anny Chantal Levasseur-Regourd,
Jean-Baptiste Renard

► **To cite this version:**

Edith Hadamcik, Jérémie Lasue, Anny Chantal Levasseur-Regourd, Jean-Baptiste Renard. Analogues of interplanetary dust particles to interpret the zodiacal light polarization. *Planetary and Space Science*, 2020, 183, pp.104527. 10.1016/j.pss.2018.04.022 . insu-01782562

HAL Id: insu-01782562

<https://insu.hal.science/insu-01782562>

Submitted on 18 Jul 2018

HAL is a multi-disciplinary open access archive for the deposit and dissemination of scientific research documents, whether they are published or not. The documents may come from teaching and research institutions in France or abroad, or from public or private research centers.

L'archive ouverte pluridisciplinaire **HAL**, est destinée au dépôt et à la diffusion de documents scientifiques de niveau recherche, publiés ou non, émanant des établissements d'enseignement et de recherche français ou étrangers, des laboratoires publics ou privés.

Accepted Manuscript

Analogues of interplanetary dust particles to interpret the zodiacal light polarization

E. Hadamcik, J. Lasue, A.C. Levasseur-Regourd, J.-B. Renard



PII: S0032-0633(17)30496-8

DOI: [10.1016/j.pss.2018.04.022](https://doi.org/10.1016/j.pss.2018.04.022)

Reference: PSS 4527

To appear in: *Planetary and Space Science*

Received Date: 26 December 2017

Revised Date: 20 April 2018

Accepted Date: 25 April 2018

Please cite this article as: Hadamcik, E., Lasue, J., Levasseur-Regourd, A.C., Renard, J.-B., Analogues of interplanetary dust particles to interpret the zodiacal light polarization, *Planetary and Space Science* (2018), doi: 10.1016/j.pss.2018.04.022.

This is a PDF file of an unedited manuscript that has been accepted for publication. As a service to our customers we are providing this early version of the manuscript. The manuscript will undergo copyediting, typesetting, and review of the resulting proof before it is published in its final form. Please note that during the production process errors may be discovered which could affect the content, and all legal disclaimers that apply to the journal pertain.

Analogues of interplanetary dust particles to interpret the zodiacal light polarization

E. Hadamcik^{1*}, J. Lasue², A.C. Levasseur-Regourd³, J.-B. Renard⁴

¹CNRS/INSU, LATMOS-IPSL, 11 bld d'Alembert, 78280 Guyancourt, France
edith.hadamcik@latmos.ipsl.fr

²IRAP, Université de Toulouse, CNES, CNRS, UPS, Toulouse, France
jeremie.lasue@irap.omp.eu

³Sorbonne Université; CNRS-INSU; LATMOS-IPSL, Campus Pierre et Marie Curie, 4 place Jussieu, 75005 Paris, France
Anny-Chantal.Levasseur-Regourd@latmos.ipsl.fr

⁴LPC2E-CNRS, Université d'Orléans, 3A avenue de la recherche scientifique, F-45071 Orléans-cedex 2, France
jbreward@cnrs-orleans.fr

Abstract

Context: Some local properties of the dust particles that build the interplanetary dust cloud may

be deduced from the light they scatter (with emphasize on their linear polarization). The ratio of organics (absorbing particles) to silicates (more transparent particles) was suggested through numerical simulations to reproduce the shape of the polarimetric phase curve and the decrease in polarization with decreasing solar distance.

Aims: Reproducing these properties, through measurements on real dust particles lifted in microgravity conditions, in the PROGRA2 light scattering experiment. Using dust analogues with parameters similar to those derived from numerical simulations.

Methods: Analogue particles, previously tested for the two main sources of dust in the inner interplanetary cloud (comets and asteroids) were used in the experiment. The ratio between fluffy aggregates and compact particles was kept constant. Five samples were studied, corresponding to mixtures with the organics / silicates ratio as defined in the numerical simulation

Results: We show that we can reproduce by experimental simulations the polarimetric properties of particles present in the inner interplanetary dust cloud, i.e. their polarimetric phase curve in the symmetry plane at 1.5 au from the Sun and variations of polarization at a 90° phase angle as a function of the solar distance between 0.5 au and 1.5 au. The effect of the different parameters suggests a size distribution of the particles following a power law with coefficients of (-3 ± 0.5) for a size-range of 10-100 μm and (-4.4 ± 0.6) for a size range of 100-200 μm , with a steep cutoff at about 10 microns, a constant ratio of (35 ± 10) % in mass of fluffy aggregates versus compact particles and a decreasing ratio of organics with decreasing solar distance. Such results are discussed in the context of recent evidence on cometary dust particles from the Rosetta mission to a Jupiter family comet.

Keywords

Interplanetary dust; cometary dust; Rosetta; light scattering; polarization; experimental simulation

1. Context of the study

In this section, we summarize properties of the interplanetary dust cloud, including the origin of its particles, their sizes distributions and their evolution. With a major contribution in the inner interplanetary cloud originating from comets, Rosetta's rendezvous mission now provides evidence on an heterogeneous population of dust particles with large (10 to 100 μm and above) particles constituting of more or less fluffy aggregates, (the wording 'compact' will be used for the denser particles), allowing us to better compare the properties of interplanetary and cometary dust particles. Before space missions to comets and asteroids, and the in-situ capture of particles, the physical properties of the interplanetary particles and their composition were mainly known when collected in the Earth vicinity. Comets and asteroids were also intensively studied by remote observations. The results (e.g. the polarization of the scattered light) were interpreted using numerical and experimental simulations. Space missions gave a ground-truth to the properties of the dust particles. These results will finally be used in the next sections to the study of the interplanetary particles and the zodiacal light.

1.1 General properties of the interplanetary dust medium

The existence of the interplanetary dust cloud was first suspected from observations of the solar light it scatters, called zodiacal light. Its glow can be observed from Earth in a plane close to the ecliptic. Around and close to the Sun, the F-corona is mainly observable from the Earth during solar eclipses or during solar occultation from spacecraft. Detailed descriptions of the zodiacal light and the properties of interplanetary dust can be found in Levasseur-Regourd and Hasegawa (1991), Leinert et al. (1998), and in Grün, et al. (2001), and references therein. Closer to the Sun than the Kuiper belt and the giant planets region, dust particles are mainly released from asteroids and from comets (Mann et al., 2006). A review of the measurements and discussion on the cometary and other contributions can be found in Sykes et al. (2004).

The dust cloud is optically thin. Some heterogeneities like dust bands from asteroidal collisions in the main asteroids families and cometary dust trails are observed (Reach et al., 2007). The particles in the dust trails are ejected by Jupiter-family comets. They were first discovered by IRAS but can also be observed in the visible (e.g. Sykes and Walker, 1992; Ishiguro et al. 2003; Agarwal et al., 2010). The trail's trajectories are close to their parent comet's orbits as the particles are usually ejected from the nucleus during previous orbits. They are dark and probably of high porosities and their sizes seem to be in a few centimeters size range (Ishiguro et al., 2002).

Complementary data were obtained for solar distances smaller than about 3 au by in situ impact measurements from space probes (Grün et al., 1985; 2001) but the number of impacts was always small and restricted to narrow size ranges. Power-law size distributions of the particles in the range from 0.1 μm to 1 cm were defined from micro-crater studies on returned lunar samples (Hörz et al., 1975; Grün et al., 2011). The flux as a function of the radius of the particles may be described by power law distributions R^{-a} , which are different for submicron-sized particles and particles larger than 20 μm . Differential size distributions for the different size ranges may be deduced from the fits on Grün's et al., (1985) figure; the differential distribution being the derivative of the cumulative distribution. In average the differential size distribution for different size ranges is found to be $R^{-3.8\pm 0.3}$ between about 0.01 μm and 1 μm , $R^{-2.6\pm 0.3}$ between about 1 μm and 10 μm , and $R^{-4.6\pm 0.2}$ between about 10 μm and 1 cm. In the

Earth's stratosphere, interplanetary dust particles, so-called IDPs may be collected (Flynn 1994; Brownlee, 2016); their size ranges from 5 to 100 μm , some of them are aggregates of micrometer-sized (or smaller) grains.

1.2 Origin of dust particles in the interplanetary cloud and their evolution

Different forces are applied to interplanetary dust particles, which induce variations in the cloud properties (Burns et al., 1979). The main forces acting on the particles are the gravity and the solar radiation pressure. The magnetic fields may also influence the distribution of dust. The dust particles spiral towards the Sun under the Poynting-Robertson drag depending on the radiation-pressure momentum. The dust particles may also fragment under mutual collisions, or evolve by sputtering and/or thermal heating with sublimation of some more volatile components or degradation of the materials close to the Sun (Mukai et al., 2001; Mann et al., 2004). Yang and Ishiguro (2018) consider that the mutual collision within the interplanetary dust cloud is ignorable, taking into account the presence of fluffy aggregates ejected by comets and also found in the Earth's stratosphere. Small particles e.g. ejected by comets or coming from the interstellar medium, are deflected out of the solar system by radiation pressure force. The expected lifetime of a typical interplanetary dust particle located at 2 au is several 10^4 years (Leinert and Grün, 1990). The usual large eccentricities of Jupiter Family Comets (JFCs) indicate dynamical lifetimes up to an order of magnitude shorter than the Poynting-Robertson drag (Yang and Ishiguro, 2018). Lasue et al. (2007) have modelled the light scattered by a cloud of particles and their equilibrium temperature, for a mixture of fluffy (supposed of cometary origin) and compact particles (supposed of asteroidal origin) made of silicates and dark organics; they suggested more than 20 % particles in mass from cometary origin. They found a size distribution between 0.2 μm and 200 μm (see section 2 for the numerical simulation results). From infrared observations and orbital considerations, a major contribution to the dust located around 1-2 au corresponds to the JFCs for 85 %, the long period comets for less than 10 %, the dust from asteroids representing less than 10 % (Nesvorný et al., 2010). These ratios may be slightly different due to differences in composition (infra-red emissions by high albedo materials being smaller than materials containing organics). A 70 % ratio of dust from cometary origin was deduced by modelling the infrared emission observed by IRAS and COBE satellites (Rowan-Robinson and May, 2013). Based on the amount of fluffy particles in Lasue et al., 2007, and considering the respective fraction of those particles to the total ejected types of particles (fluffy and compact), the contribution of comets to the interplanetary medium would be about 50 % based on 81P/Wild2 Stardust results (Hörz et al., 2006) and more than 80 % with the Rosetta results (Fulle et al., 2016).

1.3 Properties of dust particles collected by space missions and in the Earth environment

As measured from collected particles by the Stardust mission at comet 81P/Wild 2, comets eject fluffy and quite compact particles (Hörz et al., 2006) confirming deduction from remote observations and simulations (Hadamcik et al., 2006; 2009b; Lasue and Lévassieur-Regourd, 2006; Lasue et al., 2009). Images of both types of particles were obtained by the COSIMA instrument on board Rosetta (e.g. Schulz et al., 2015; Langevin et al., 2016; 2017) in the coma of comet 67P/Churyumov-Gerasimenko (thereafter 67P). Similarly, MIDAS, Rosetta's atomic force microscope, measured the shape, size and texture of the collected particles demonstrating a hierarchical building of the dust aggregates (Bentley et al., 2006). Ultra-

carbonaceous-meteorites collected in the ices of Antarctic, are rich in organics and porous. They are supposed to be of cometary origin based on their composition and structure (Engrand and Maurette, 1998; Dobrica et al., 2012). In addition to particles from comets, the surface of asteroids covered by regolith may also produce very fluffy debris. Figure 1 presents example illustrations of IDPs and cometary particles.

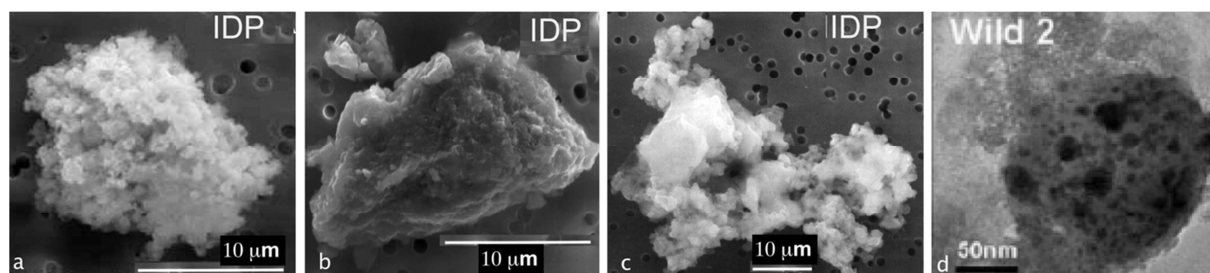


Figure 1. SEM images (NASA) of three IDPs particles (a,b,c) collected in the upper Earth atmosphere, one dust particle from comet Wild 2 (Zolensky et al., 2006) (d).

Very large particles (more than 1 mm) were observed before perihelion by OSIRIS and GIADA experiments on board Rosetta in the inner coma of 67P. The size distribution changed with perihelion distance with an increase of small particles close to perihelion. The particles were dark, numerous particles were fluffy aggregates and others were denser, as the particles collected by COSIMA with a resolution of 14 µm (Langevin et al., 2016, 2017) and the analysis of the impacts from GIADA and the scattered light by OSIRIS (Rotundi et al., 2015; Fulle et al., 2016; Fulle and Blum, 2017). MIDAS analyzed particles in the (1-10) µm range with a resolution down to nanometers and found aggregates with different structures at different scales; one of them was very porous, with a fractal dimension of about 1.7 (Bentley et al., 2016; Mannel et al., 2016). These results represent a ground truth for cometary particles even if particles ejected by other comets could be different (e.g. comet C/1995 O1 Hale-Bopp or 81P/Wild 2, Wooden et al., 2017).

1.4 Composition of interplanetary dust particles

The two main components of the dust particles collected in the stratosphere are minerals (mainly silicates) and complex refractory organics. Their precise composition (relative ratio of different elements, structure of the grains in the particles) can give some insight on their origin in the early solar system. The main technique to access their composition is remote or in-situ infrared spectroscopy compared to laboratory studies of collected particles (Hanner and Bradley, 2004 and references therein; Wooden et al., 2017). Cometary dust represents an un-equilibrated, heterogeneous mixture of crystalline and glassy or amorphous silicate minerals, organic refractory materials, and other constituents such as iron sulphide and possibly minor amount of iron oxides. The composition of the particles on the surface of asteroids is mainly obtained by telescopic reflectance spectra from Earth or from space probes, and infrared spectra obtained in the laboratory showing that some IDPs are coming from very primitive asteroids (types P and D) and present characteristics reminiscent of cometary dust particles (Vernazza et al., 2015). Mineralogical studies of IDPs have also shown some possible links with some meteorites and C-types asteroids for a minor portion of the collection (Keller et al., 1992; Thomas et al., 1995). In IDPs, organic mantles were found on grains (Flynn et al., 2013), confirming the suggestion made by Greenberg and Hage (1990) of organics coating of interstellar grains before the planetary accretion but in the numerous IDPs they are probably uncommon. Amorphous minerals (silicates, sulphides, metals) may be

embedded in the organics, or just mixed to them making their relationship difficult to disentangle.

1.5 Observations of the solar light scattered by dust particles

Observations of the light scattered by the particles at different wavelengths and its linear polarization allow to infer some of their properties (size and size distribution, morphology and structure, refractive indices and thus composition and albedos). In remote observations, asteroids are quasi-stellar objects and cometary comae are relatively small objects. The dust particles are therefore seen under a given phase angle. On the opposite, the interplanetary dust producing the zodiacal light is an extended source and the observed scattered light changes along the line of sight (see e.g. Fig. 24.2 in Lasue et al., 2015). To retrieve the local dust properties, inversion of the data is necessary, whenever possible. Local intensities, albedo, color and linear polarization have been obtained, through the use of a lesser uncertainty method, in specific locations: as a function of the phase angle in the symmetry plane (close to the ecliptic) at a solar distance of about 1.5 au and at a phase angle of 90° as a function of the solar distance (Dumont and Levasseur-Regourd, 1988; Renard et al., 1995; Levasseur-Regourd et al., 2001; Lasue et al., 2015 and references therein). From the ultraviolet domain ($\lambda > 0.2 \mu\text{m}$) to the near-infrared domain ($\lambda < 2 \mu\text{m}$), the spectral properties of the light are dominated by the solar scattered light (Leinert, 1975 and references therein; Kawara et al., 2017). The polarization phase curve (polarization as a function of the phase angle) for atmosphere-less objects (i.e. asteroids) and clouds (cometary comae and interplanetary dust cloud) have similar shapes indicating the presence of irregular particles, with a positive branch and a maximum polarization P_{max} close to a phase angle of 90° , a shallow negative branch with a so-called minimum polarization P_{min} and an inversion angle α_0 (e.g. Fig. 1 in Hadamcik et al., 2006). The other parameters are the slope “h” at inversion (transition zone from negative to positive polarization) and the phase angles at minimum and maximum polarization.

The polarization properties of the light scattered by dust in the interplanetary dust cloud are summarized and reviewed in Lasue et al., 2015. The inversion of data for light scattering observations has been, up to now, mostly possible in the symmetry plane (close to the ecliptic plane) between 0.3 and 1.5 au from the Sun. In the whole region, the inversion gives access to the local polarization at a phase angle of 90° as a function of the solar distance R and at a heliocentric distance of 1.5 au as a function of the phase (Fig. 6). Intensity, albedo and temperature of the grains were also retrieved (Dumont and Levasseur-Regourd, 1988; Renard et al., 1995; Dumont et al., 1998; Levasseur-Regourd et al., 2001). The local albedo of the dust cloud increases, approximately following a power law distribution: $A = (0.07 \pm 0.03) R^{0.34 \pm 0.05}$ in the near ecliptic symmetry plane as a function of the solar distance, R , between 1.5 au and 0.5 au as deduced from the brightness derived local properties. The local polarization phase curve, at 1.5 au from the Sun in the symmetry plane presents a well-developed positive branch, and a maximum polarization of about $30\% \pm 3\%$ at 90° phase angle and a shallow negative branch in the back scattering region ($P_{\text{min}} = -1\% \pm 0.05\%$ at $\alpha_{\text{min}} = 7.5^\circ \pm 1^\circ$), with an inversion angle $\alpha_0 = (15 \pm 2)^\circ$. At 90° phase angle, the local polarization was derived at different solar distances (Levasseur-Regourd et al., 1999). A decrease in polarization P can be noticed between 1.5 au and 0.5 au at $\alpha = 90^\circ$ (Lumme 2000; Levasseur-Regourd et al. 2001) with $P_{90^\circ}(\%) = (30 \pm 3) R^{0.5 \pm 0.1}$. For solar distances between 0.4 au and 0.2 au, P is practically constant and decreases drastically for solar distances smaller than 0.2 au in the solar F-corona, suggesting drastic changes of the dust properties in terms of composition and/or size distribution in this region (Mann et al., 2004). The spectral gradient in polarization if any, is small but may be negative in the near infrared (Leinert et al., 1998). The local temperature of

the grains increases when the solar distance decreases. Between about 1.5 au and 0.5 au it approximately follows a power law (less steep than that of a black body): $T = (250 \text{ K} \pm 10 \text{ K}) R^{-0.36 \pm 0.03}$ (Dumont and Levasseur-Regourd, 1988; Reach, 1991; Renard et al., 1995; Levasseur-Regourd et al., 2001). This temperature increase may play a role in the change in the properties of the organics as it facilitates the sublimation or transformation of some of them.

A comparison of phase curves between comets, asteroids and the interplanetary dust cloud can be found in Hadamcik et al. (2009a) showing two classes of comets and different asteroid types. Some results are given below. Remote observations of dust, with fluxes integrated on a relatively large aperture allowed to reveal different classes of comets by their polarimetric properties (Levasseur-Regourd et al., 1996; Levasseur-Regourd & Hadamcik, 2003a; Kiselev et al., 2015). The main differences between these classes is the maximum polarization value at about 90° phase angle. The phase functions (intensity and polarization) depend on the wavelength of observations; usually cometary dust is redder than the solar light and its polarization presents a positive spectral gradient. The dust albedo is low, the absorption being mainly the results of carbon-bearing materials. The two classes of comets are confirmed by the thermal properties, with a correlation between higher polarization, stronger infrared silicate emission and higher infrared color temperatures (Hanner, 2003; Kolokolova et al., 2007). The comets are generally observed in the inner solar system region, where the solar heating may induce a high activity. Imaging polarimetry had also allowed characterizing different regions in the coma indicating different physical properties for the particles (Renard et al., 1996; Hadamcik and Levasseur-Regourd, 2003a; 2003b; 2016). For the same comet, an evolution of the particles properties is also observed as a function of the solar distance (difference before and after perihelion as observed in the coma of 67P, Hadamcik et al., 2017) and confirmed by the ejection of smaller particles at perihelion in the Rosetta observations (Della Corte et al., 2016; Fulle et al., 2016).

Before the choice of cometary analogues, systematic studies of the variations of polarization with the physical properties of the dust, such as size, porosity, or albedo for the different kinds of particles (fluffy or more compact), transparent or absorbing were studied with the PROGRA2 experiment (Section 3) to interpret remote-sensing observations of comets; they also allowed to study the influence of interconnection between sizes (aggregates and grains) and absorption on the amplitude of the positive branch (Hadamcik et al., 2009; Hadamcik et al., 2011a; Levasseur-Regourd et al., 2015). Cometary analogues made of a well-homogenized mixture of Mg-Fe-silicates (average constituent grain 50 nm) with carbon-black (constituent grain 14 nm) were suggested. The amplitude of the positive branch (P_{max}) was too large for whole coma polarization, it was adapted to the coma of comet Hale-Bopp or to the jets of ordinary comets. Some denser with coarser grains silicate particles were necessary to obtain a good analogue for other cometary phase curves

Different taxonomic classes of asteroids have been defined by studying their reflectance spectra (Tholen et al., 1989; Bus and Binzel, 2002; DeMeo et al., 2009). The porosity of the surface allows to observe emission features in the mid-infrared domain (Vernazza et al., 2012). Linear polarization observations have confirmed a correlation between the taxonomic classes and the polarimetric phase curves (Goidet-Devel et al., 1995; Penttila et al., 2005; Cellino et al. review, 2015). This correlation is related to the composition and surface structure. Meteorites are collected on Earth or spacecraft and studied in laboratory, for many of them their parent body is an asteroid (only its class is known). Some asteroids have been observed to disrupt on impact and others to disintegrate probably due to rotationally induced break up (Jewitt et al., 2010; 2014). These are relatively rare events, but the ejected dust and related trails may be observed. A review of the so-called active asteroids can be found in

Jewitt et al. (2015) and references therein. The polarimetric phase curves of pulverized meteorites deposited on a layer were studied and compared to asteroidal phase curves (Hadamcik et al., 2011b). Some meteorite classes seemed to be linked to M- and C-types asteroids. Pulverized meteorites are used as asteroidal analogues with the cometary analogues to build the interplanetary dust cloud analogues. Nevertheless, some cometary analogues can be also considered as asteroidal analogues (i.e. compact silicates, basalt, lignite coal). On the other hand, it is sometimes difficult to disentangle the two populations of objects; asteroids were also observed on comet-like orbits, 80 % of them have low-albedo consistent with the properties of comet nuclei (Kim et al., 2014). Similarly DeMeo and Binzel showed that (16 ± 5) % of the population of near-Earth objects have comet-like dynamical and physical properties.

Local polarimetric results are derived from the observations and a numerical simulation of the scattered light and its linear polarization are presented in section 2. In section 3, using these results, experimental simulations were performed with the Propriétés Optiques des Grains Astronomiques et Atmosphériques (PROGRA2) experiment, with particles lifted in microgravity conditions (Worms et al., 1999; Renard et al., 2002; Levasseur-Regourd et al., 2015). To choose analogues for the simulations, it was necessary to derive the average composition of the dust, the size distribution of the particles and their structure. Some analogues were previously suggested for different sources (comets, asteroids) and their light scattering results compared to remote and in situ observations (e.g. Hadamcik et al., 2007a; 2011). The structure and the size range of the samples used in the experiment are presented in section 3 for different mixtures; the experimental results obtained for the polarimetric phase curves are compared to observations and numerical simulation of local polarization at 1.5 au in the symmetry plane together with the variation of maximum polarization at 90° phase angle as a function of the solar distance. In section 4, the choice of the dust particles is discussed. Some examples taken from cometary results and experimental simulations are proposed for disintegration of organics with their temperature increasing when closer to the Sun. The study of an olivine sample proposed as possible cosmic dust or cometary dust analogue by polarization studies is also discussed. In section 5, the main conclusions of the present study are summarized.

2. Numerical simulations for the inner interplanetary dust polarimetric observations (LLFCmodel2007)

The results obtained in Lasue et al. (2007) numerical model (hereafter noted LLFCmodel2007) were used to tentatively interpret the local properties deduced by inversion of the observations. To fit the data, the relation giving the polarization at 90° phase angle as a function of the heliocentric distance was used (section 1.5). The model is shortly described here to help explain the choices made for the experimental studies. The model particles were first used for simulations of cometary coma particles (Lasue & Levasseur-Regourd, 2006; Lasue et al., 2009). They were either compact and/or fluffy aggregates. To avoid resonances due to spherical particles (Mie scattering), compact particles and grains were described as spheroids in different orientations. Aggregates of grains were fractal. The equivalent size of the particles was the radius of a sphere of equivalent volume of material. If the density was the same for all the grains of one kind of materials, their volume fraction was proportional to the mass of the particles. To decrease the number of parameters, the silicates were described by one complex refractive index corresponding to Mg-rich pyroxenes ($m = 1.62 + i0.03$) and the organics were described by a refractive index $1.88 + i0.1$ close to those of amorphous carbon (or soot) particles. Some grains were only made of silicates. The organics were deposited on silicates in thick mantles. The width of the mantle was sufficiently large (at least

for the largest grains) to avoid any effect of the core silicates i.e. the light scattered by such particles was similar to light scattered by organics only, producing an uncertainty on the organics over silicates ratio. The size distributions, for different size ranges, were taken from Grün et al. (1985; 2001). Similar measurements on Grün's et al. (1985) fits were adapted to model the experiment size ranges to build the analogue cloud for light scattering studies.

For the LLFCmodel2007, a power-law coefficient of -3 for particles smaller than 10 μm and -4.4 for particles in the 10-100 μm range were adopted (approximately consistent with Grün et al., 1985). The largest particles had a small influence on the scattered light. To calculate the polarimetric phase curve at 1.5 au, the derived local properties data were averaged for each phase angle. Taking into account thermal considerations, model values were deduced from the derived local properties data set at 90° phase angle as a function of the solar distance between 0.4 and 1.5 au. To fit the data, the ratio between aggregates and compact particles was kept constant and the ratio of organics over silicates decreased. Because one cannot differentiate between particles with a thick organics coating and pure organics particles, the results are given by two different organics to silicates ratios (the smaller one when considering a silicate core covered in organics and the larger limit when the dark particles are considered to be made of pure organics). The best fit was obtained with 20 % to 60 % organics for a size distribution between 0.22 and 20 microns. Fractal aggregates were estimated to contribute at least 20 % in mass of the dust cloud at 1.5 au. A different approach, relying on modelling of both the light scattering and thermal properties of aggregates of larger grains, has also been leading to the presence of compact and fluffy particles, with composition ranging from silicates and more absorbing materials (Levasseur-Regourd et al., 2007).

3. Experimental simulations

To help to interpret the polarimetric observations in terms of physical properties of the particles, different analogues including very large fluffy and more compact particles are suggested for dust particles in the interplanetary dust cloud. Such particles which corresponds to analogues for cometary comae dust were studied with the PROGRA2 experiment either in microgravity conditions or with particles lifted by an air draught (when the particles are of high porosities and/or smaller than 20 μm); the results were compared to remote polarimetric observations for specific comets: e.g. comet C/1995 O1 Hale-Bopp, comet 103P/Hartley 2, comet 67P/Churyumov-Gerasimenko (Hadamcik & Levasseur-Regourd, 2003b; Hadamcik et al., 2013; 2017).

3.1 Experiment

The studied samples for the present experimental simulations are mixtures of compact and fluffy particles with large size distributions. To avoid segregation by weight, the levitation of the sample was obtained during parabolic flights onboard the A300 ZeroG aircraft, which provide microgravity conditions. The aircraft was operated by the Novespace company during campaigns funded by the French space agency CNES and the European space agency ESA. The measurements of the light scattered by the samples are obtained by the imaging polarimeter PROGRA2-vis (vis is for visible domain); the principle of measurements is presented in Figure 2; the technical details can be found in Renard et al. (2002) and Hadamcik et al. (2009a). The optical fiber is fixed on the vial which rotate with its stand, allowing to change the phase angle. The random polarization is verified at each microgravity campaign. The error bars produced by the system of lasers and receptors are typically between 1 and 2 % depending on the scattered flux by the particles, they are calculated from the dispersion of the

flux on the individual images. The spatial resolution of the polarized images taken by PROGRA2 is of 20 μm .

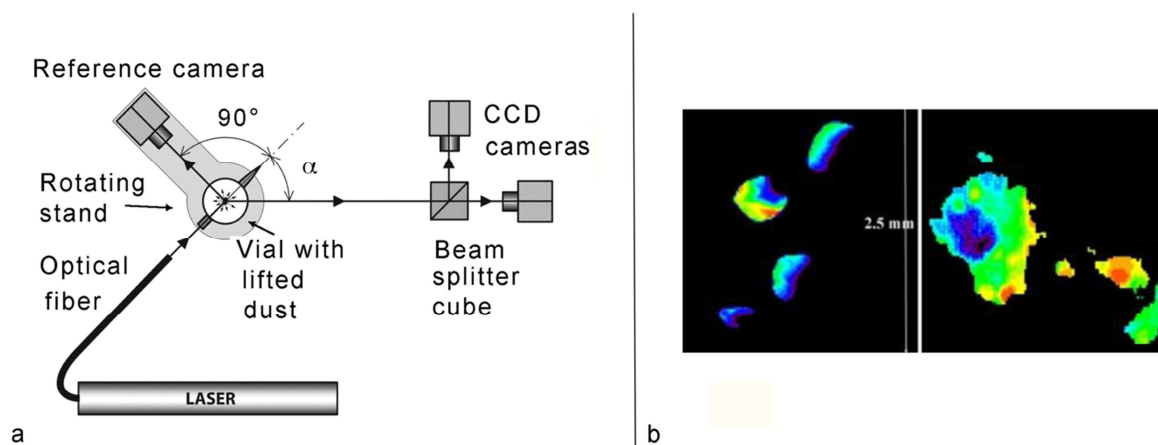


Figure 2. a: Schematic view of the PROGRA2-vis instrument (α is the phase angle). b: example of image recorded for a phase angle of 90° ; on the polarization maps: left, aubrite meteorite particles are compact; right, silica particles are fluffy. On the images the light source is on the left; the yellow color is for bright regions, the blue ones for dark regions. The color on the images gives some idea on the shape of the particles. Adapted from Hadamcik et al., 2011a.

The reference camera performs measurements at a constant phase angle of 90° whatever the observed phase angle by the cameras; in the present study, it allows to control the particles number and size in the beam. In the vial, the dust mass for these experiments was about 0.3 g for each sample. The particles in the field of view are compact large particles or agglomerates of the materials mainly with small grains and aggregates.

3.2 Samples

We work with real particles and try to make the mixtures of particles to correlate with the remote-sensing derived local properties of the zodiacal cloud and the numerical simulations results, using our cometary analogues samples and pulverized meteorites as asteroidal analogues. On Figures 3, 4, 5 SEM and TEM images of samples are presented, some of them in two scales showing aggregated structures.

3.2.1 Minerals

Materials are fluffy aggregates of un-equilibrated Mg-silicates and Fe-silicates composed of submicron-sized constituent grains (Hadamcik et al. 2007a), aggregates composed of micron- to 10 micron-sized constituent grains: amorphous enstatite and forsterite, some were heated to obtain crystalline grains, fluffy silica with 40 nm constituent grains (fractal type) and low-density silica produced by random ballistic deposition (Blum and Schr apler, 2004; Hadamcik et al., 2007b), pulverized basalt from the seabeds, meteorites (aubrite and CO3-chondrite), the CO3 sample with less than 1 % carbon in mass (Pearson et al., 2006). Figure 3 shows three rock forming samples. Figure 4 shows two crushed meteorites dust at different scales; they seem to be compact but their fine structure is often porous. The meteorites are more specifically chosen as asteroidal components but other minerals may also be analogues for different asteroid types. In the captions of Table 1, the corresponding 'materials' were added as (T1.x).

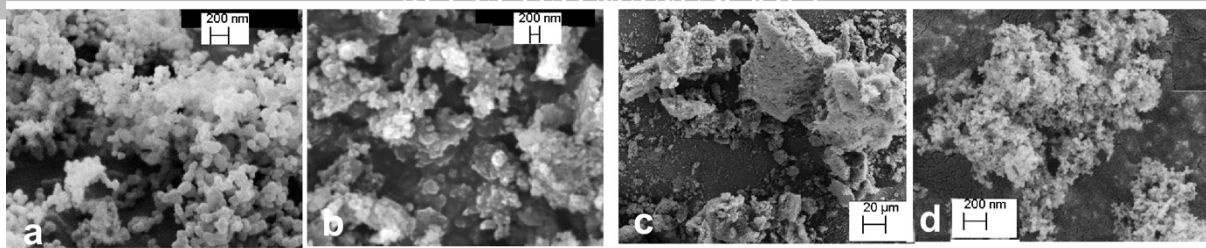


Figure 3. SEM images of some silicate samples. a. Mg-Silicate with in average 50 nm constituent grains in fluffy aggregates (T1.a). b. Enstatite (Mg-silicate), compact particles with some crystals and aggregates with constituent grains in a 100 nm-10 μm range (T1.b). c. Fe-silicates, fluffy aggregates with grains coated by organics (T1.c). d. Same as c, but showing the constituent grains in the 50 nm size-range.

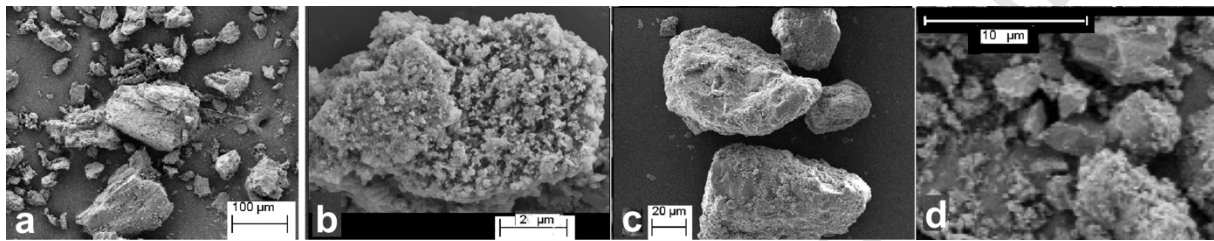


Figure 4. SEM images of pulverized meteorites used to compare their polarimetric phase curves to asteroidal and to cometary ones. a & b: aubrite (T1e), c & d: CO₃-chondrite type (T1f). For each sample, two scales are presented, a & c: with an apparent compact structure with different porosities, b & d: aggregated grains in the particles.

3.2.2 Organics

The main materials are carbon-black aggregates with 14 nm and 95 nm constituent grains, coal of low maturity (pulverized lignite with micron to 100 micron-sized relatively porous material) and some fluffy C_xH_yN_z (in average 100 nm grains) of different composition (poly-HCN and various tholins produced in a CH₄-N₂ gas phase of radio frequency plasmas). In these last samples, the ratio N/C is comparable to the results obtained for 1P/Halley and by COSIMA/Rosetta in solid organics (hereafter CC for organics or carbonaceous-compounds), it is higher than in carbonaceous chondrites (Fray et al., 2017). Figure 5 presents two carbon samples: the carbon-blacks are fluffy, with fractal-type arrangements and lignite is a coal, it is compact but porous.

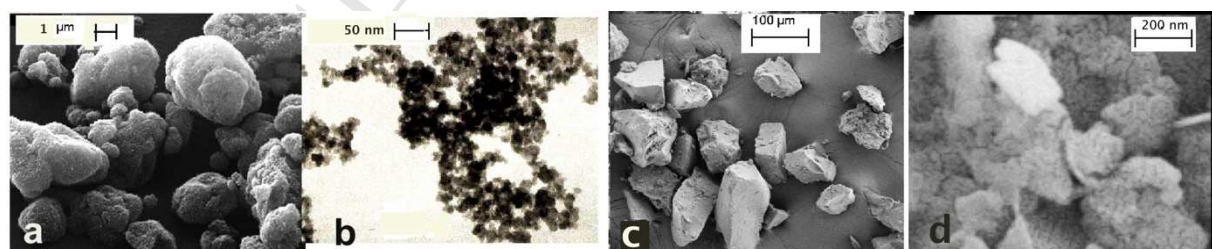


Figure 5. Carbon samples. a. SEM image of fluffy aggregates of carbon-black (T1.h); b. TEM image of the carbon-black showing the chains with grains (fractal type) (T1.h). c & d SEM images of lignite at two different magnifications (T1.l).

Five samples were prepared by mixing the different materials. Table 1 gives the main components and their structures.

Materials	Fluffy Aggregates size range of their grains	Compact particles	Figures number	Analogues
(a) un-equilibrated Mg-silicates	- average size 50 nm		3a	Comets
(b) enstatite and forsterite with crystals or not		size range (50-300) μm and crystals in a 1 μm range	3b	Comets
(c) basalt		- size range (5-75) μm	-	Comets or asteroids
(d) Fe-silicates (coated by CC)	- average size 40 nm		3c-3d	Comets
(e) Saharian aubrite meteorite			4a- 4b	Asteroids
(f) CO3 meteorite			4c-4d	Asteroids
(g) Silica	-(g1) average size 14 nm -(g2) average size 40 nm -(g3) size range (1-5) μm		- - -	Comets Comets Comets
Organics (CC)				
(h) Carbon black	- average size 14 nm		5a-5b	Comets
(i) Carbon black	- average size 95 nm		5a-5b	Comets
(j) poly-HCN	-(j1) size range (0.1-1 μm)	(j2) size range (10-100) μm	-	Comets
(k) tholins (C _x H _y N _z)	- average size 200 nm		-	Comets
(l) coal (lignite)		size range(20-100) μm	5c-5d	Comets

Table 1. Structure and size range of the materials. In the last column, the Figure number is indicated for the samples when presented in the paper. Cometary or asteroidal analogues when previously used with the experiment are specified.

3.3 Size distribution

The size distribution of the compact grains was measured on SEM images. For large compact particles, the size can be measured on the polarization maps built from the PROGRA2 cameras images. The size of the large agglomerates, which are made of small compact grains and/or of small aggregates, is also measured on the polarization images.

To adapt the size distribution measured in the experiment (equivalent diameter of the projected surface) to the size distribution in mass in LLFCmodel2007, the effective size of the particles has been calculated. A rough porosity of the agglomerates made of the fluffy particles of silica and carbon-black was estimated from volume and mass measurements made in a box of 15 x 6 x 5 cm³, where the fluffy particles were just sprinkled, without any compression. An analysis of the intensity by pixel in the PROGRA2 image of the particles gives indication on the structure of the particles, whether they are aggregated or compact. The edge of each particle in the image seems to be blurred for aggregates, while compact particles have sharper edges (Fig.2, right). In a first approximation, the agglomerates in each size range were supposed to have 80-90 % porosity (which is a very rough average value, the agglomerates made by agglomeration from smaller aggregates and grains are not homogeneous). In these conditions, the effective diameter of the agglomerates was about half of the one measured in the PROGRA2 images. This first correction was applied to determine the effective size distribution in mass of real particles floating in micro-gravity.

The ratio between dark particles and transparent ones also needs to be estimated. The dark particles are not always detected by the PROGRA2 cameras. When they are small, their projected surface area could be smaller than the actual one. Therefore, the size distribution of the detected particles is underestimated with respect to the actual size distribution of the particles in the vial. A corrective coefficient needs to be applied on the number of particles in the size ranges of 20 and 30 μm when transparent and absorbing particles are mixed. Their

values were evaluated with the experiment for the different materials. Aggregates with constituent grains larger than 5 μm , were considered as compact particles. In the first four mixtures, with a relatively high ratio of carbonaceous particles which are absorbing, a corrective coefficient is applied for small particles at the limit of the instrument resolution (20 μm), after tests on calibrated samples. The corrections are described below. A sample is defined by its silicates over carbon ratio, its size distribution and ratio of aggregates over compact structures (Table 2).

A mixture of minerals (materials 'T1.a-d-g' for the aggregates and 'T1.b-e-f-g' for compact particles from Table 1) is first realized, representing (35 \pm 10) % aggregates and (65 \pm 10) % compact. The ratios of each mineral are the same for all the final mixtures. CO3 meteorite material (T1.f) contains less than 1 % CC (taken into account in the calculations). No reason was found to change the materials and their ratios in the present work, except between mixture 1 and 2 for which 'T1.g1' is taken for mixture 1 (smaller grains in aggregates) and 'T1.g2' for mixture 2. The same quantities are taken to finalize the mixtures. The total mass for the CC are calculated from the silicate total mass to represent 60 %, 40 % and 30 % of the mixtures. The ratios between compact and aggregates are calculated to provide the needed mass for each compound. The materials chosen in the two categories are the same for all the mixtures (aggregates 'T1.h-i-j1-g', compact 'j2 and j1'), except for carbon-black 'T1.h' in mixture 1 and 'T1.I' in mixture 2 (smaller grains in aggregates).

Mixtures 1 and 2 are composed of about 60 % CC (including amorphous carbon) containing fluffy aggregates: - smaller constituent grains in aggregates (14 nm-40 nm) in mixture 1, and larger ones (40 nm -95 nm) in mixture 2. The number of particles counted by the system with a diameter of 20 μm has to be increased by 40 % and the 30 μm particles has to be increased by 30 %. For largest particles, a correction is not necessary, the change of the albedo is detectable in the intensity by pixel for each sufficiently large particle.

Mixture 3: about 40 % CC, and the constituent grains size in aggregates are about the same than in mixture 2. The number of particles of 20 μm has to be increased by 30 % and by about 20 % for 30 μm particles.

Mixture 4 is composed of about 30 % CC but with less carbon-black material that is mainly coating the large compact silicate grains, and more coal (lignite). The number of particles of 20 μm has to be increased by 20 % and by about 10 % for those of 30 μm .

Mixture 5 is composed of less than 0.1 % CC (related to the total mass, it is less than 1 % in CO3 meteorite). The differences in albedo between the particles being relatively small, size distribution correction were not applied.

For each mixture, the size distribution of the constituent grains in aggregates and of the compact particles size was measured from the SEM. The ratio between 10 μm -sized particles and 100 μm particles have then been estimated, giving values between 200 and 300. The number of 10 μm particles (not detected on the experiment images) was estimated to a factor of 300 higher than the 100 μm . Between the 10 μm and 20 μm particles, a ratio of 2 was found on the SEM images. One can notice that numerous small grains and aggregates stick on the large compact particles, but it is impossible to correct this effect (seen on SEM images). Some particles agglomerate during the levitation (produced during parabolic flights) and may de-agglomerate when hitting the vial walls. Finally, a total number of 10000 particles detected by PROGRA2 was considered. The size ranges for each mixture are given in Table 2.

On average for all the mixtures, the power law index is of -3.1 ± 0.5 for a size range in the (10-100) μm , and is -4.4 ± 0.6 for a size range in the (100-200) μm . For sizes larger than 500 μm , the slope is very large, between -6 and -9, creating a cut-off for large particles (PROGRA2 was not designed to observe particles greater than several hundred of μm).

Samples	Size range (μm)	Power law index
Mixture 1	10 -120	-3.6 ± 0.2
60% CC	100-240	-5.3 ± 0.4
Mixture 2	10-100	-3.0 ± 0.25
60% CC	100-190	-4.2 ± 0.2
Mixture 3	20-70	-3.1 ± 0.1
40% CC	70-240	-4.7 ± 0.3
	>250	>-6
Mixture 4	10-100	-2.5 ± 0.1
30% CC	100-300	-3.8 ± 0.3
Mixture 5 (only minerals)	10-20	-2.8 ± 0.3
<0.1 % CC	20-100	-3.3 ± 0.2
	100-320	-4.1 ± 0.4

Table 2. Average size distributions from the experimental measurements, after corrections. The error bars are the average standard deviations for each size ranges in the different mixtures.

3.4 Results

For each sample, measurements were obtained for red and green wavelengths, during three parabolic flight sessions representing fourteen phase curves. Between the green and red wavelength domains, the difference was smaller than the error bars. In consequence, at each phase angle the data were averaged.

The experimental results are compared with the observations, the local properties inversions and the numerical simulations. Numerical simulations were obtained for solar distances between 0.5 and 1.5 au, with a phase curve in the symmetry plane at 1.5 au and the variation of polarization at 90° phase angle as a function of the solar distance (derived local properties data from: Levasseur-Regourd 1996, based on observations from Dumont and Sanchez 1975; Fechtig et al., 1981; Levasseur-Regourd et al., 1991).

3.4.1 Phase curves at 1.5 au in the symmetry plane

The experimental phase curves obtained for the five samples are superimposed to the data resulting from local inversion of polarimetric observations of interplanetary dust (Levasseur-Regourd, 1996) and to the phase curve obtained by LLFCmodel2007 (Fig. 6a). The best agreement between derived local properties from observations at 1.5 au in the symmetry plane and experimental simulations was realized for mixture 3 with $(40 \pm 5) \%$ CC and $(60 \pm 5) \%$ minerals, mainly silicates. The ratio of organics over silicates in LLFCmodel2007 was also close to 40 % which is in excellent agreement with the experimental simulation. Figure 6b is a zoom of the small phase angles region, with mixture 3 data compared to observations and presenting here also a very good agreement.

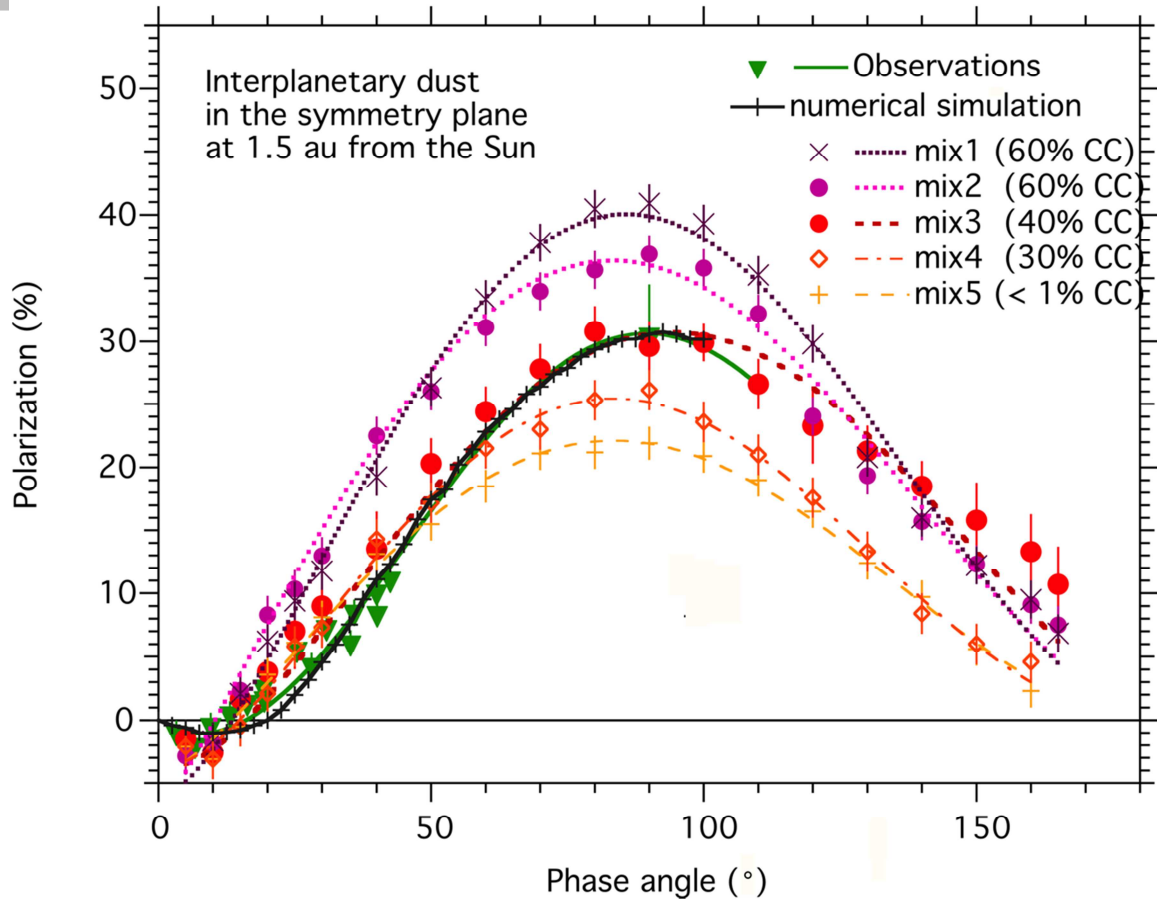


Figure 6a. Comparison of the phase curves obtained with the five different mixtures to numerical simulations and local properties derived by inversion of the observations. Best fit corresponds to 40 % of organics.

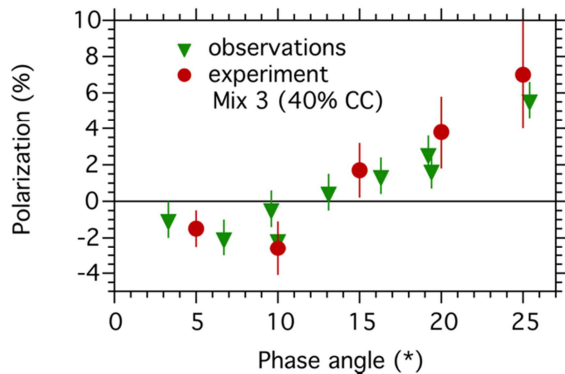


Figure 6b. Zoom of the small phase angles region, to compare observational and experimental data for 40 % CC (Mix 3).

Table 3 compares the main parameters of the three fits (local derived observational data, numerical and experimental simulations). As far as the phase curves parameters are concerned, an excellent agreement is obtained at maximum polarization between the three curves. At inversion, the agreement is good between experiment and local derived observational data despite the large error bars at small phase angles in the experimental data. The slopes at inversion and the minimum polarization value also agree, taking into account the experimental data dispersion. In fact, the uncertainties at small angles are usually higher than at other angles, because the measurements are more difficult to conduct due to the geometry of observations. Thus, the data could be more scattered. Moreover, an error bar of 1 % in polarization at phase angles larger than 30° allows usually to fit the data correctly; the

same error bar at small phase angles where the polarization is of -1 or -2 % would need numerous measurements to retrieve correct value by statistics (this is not possible in microgravity flights). Fig. 6b shows the scatter of the experimental data at such phase angles range with a relatively good agreement with the data derived from observations (in the limit of the respective error bars).

Parameters	α_{\max} ($^{\circ}$)	P_{\max} (%)	α_0 ($^{\circ}$)	h (%/ $^{\circ}$)	α_{\min} ($^{\circ}$)	P_{\min} (%)
Derived local properties	90 ± 3	30 ± 0.5	15 ± 2	0.24 ± 0.15	7.5 ± 1	-1.0 ± 0.05
Numerical model	92 ± 3	30.5 ± 0.5	20	0.15	7.5	-1
Experimental simulations	94 ± 3	30.5 ± 1.0	16 ± 5	0.45 ± 0.25	8 ± 2	-2.5 ± 1

Table 3. Parameters of the phase curves fitting the local properties deduced from observations, the numerical model and the experimental simulations.

3.4.2 Polarization at $\alpha=90^{\circ}$ at different solar distances

Figure 7 represents the polarization at about 90° phase angle (maximum on the polarimetric phase curves) as a function of the heliocentric distance. The trends for the mixtures prepared with different ratios of CC are in perfect agreement with the local properties deduced from observations and with the numerical simulations down to 0.5 au. For solar distances smaller than 0.2 au, the polarization decreases considerably, probably indicating significant changes in the particles composition but also fragmentation with eventually sublimation of silicates (Mann et al., 2004). Mixture 1 maximum polarization as compared to data at 1.5 au with a 60 % CC is slightly too large. The reason seems to be due to the too small size of the constituent grains in the aggregates. Mixture 2 maximum polarization corresponds to the results obtained by the numerical simulations at 1.5 au with a 60 % CC. Mixture 3 which contained 40 % CC, represents the best agreement with the observations if the phase curves at 1.5 au are considered. It is also in excellent agreement with data and numerical simulations at about 1 au. Mixture 4 (30 % CC) and mixture 5 (less than 1 % CC) are respectively in agreement with data at 0.8 and 0.5 au derived local properties and model.

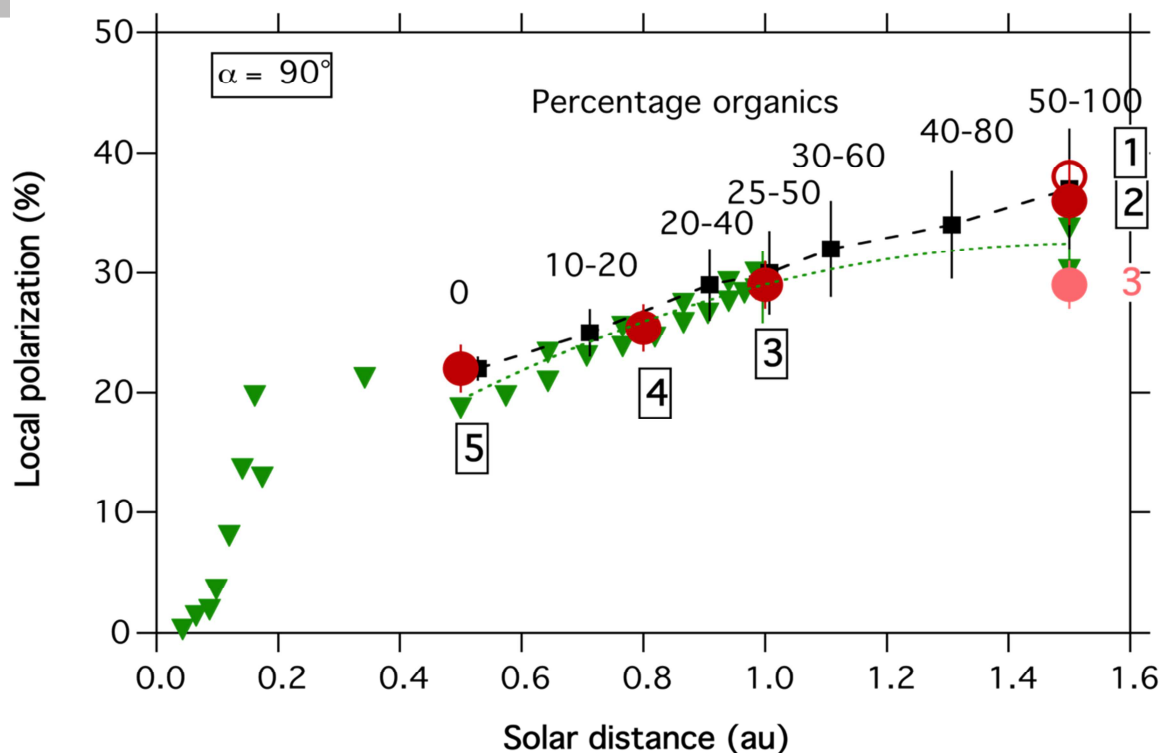


Figure 7. Experimental results (red discs and red circle) for the 5 samples as a function of the organics ratios at different solar distances between 0.5 au and 1.5 au, where numbers correspond to the mixtures as defined in Table 2; the P_{\max} values are from Fig. 6 (mix 3 ‘red symbol’ is comparable to P_{\max} at 1 au with 40 % organics, but is also comparable to local P at 1.5 au ‘clear red symbol’). Local polarization inferred from inversion of observations in the symmetry plane (green triangles), together with a fit of data between 0.5 au and 1.5 au (dotted green line). Error bars on the local polarization and the experimental results may be smaller than the symbols. At 1.5 au the error bars for the local polarization values are of $\pm 3\%$. Numerical simulations: black squares and dashed line.

4. Discussion

4.1 Interplanetary, cometary and asteroidal dust particles analogues

Cometary dust particles are a major component of the interplanetary dust, for which interpretations of remote observations have progressively been proposed with the help of numerical and experimental simulations. Asteroidal dust particles can present some similarities with them, at least when primitive asteroids are considered; C-type asteroids typically present a low albedo, probably a high porosity (Housen et al., 1999; Kuroda et al., 2017) and a phase curve similar to comets (Hadamcik et al., 2009a). The composition of the samples in the experimental simulations with mixture of silicates, carbon-black and coal for the CC, low albedo of the particles (Hadamcik et al., 2007a) is consistent with the Rosetta findings for cometary dust properties revealing the presence of numerous complex organics (Fray et al., 2016), in very large particles made of sub-micron sized grains in aggregates either compact or with very high porosities (Langevin et al., 2016; Mannel et al., 2016). Taking into account the large variety of CC found by Rosetta, some materials such as poly-HCN, or $C_xH_yN_z$ compounds and Fe-silicate coated by organics were added to the mixtures. These compounds were the same in the five samples, the amorphous carbon (C-black and lignite ratios are used for the adjustments of CC ratios) Different ‘compact’ particles used in the

cometary analogues can eventually be also used as asteroidal ones in complement of pulverized meteorites (one of them being a stony achondrite (aubrite) and the other one a carbonaceous chondrite (CO3 meteorite)).

4.2 Differences and similitudes between the numerical (LLFCmodel2007) and experimental simulations

In this section, the main parameters for each model numerical or experimental are compared (respectively same subsection letter a-a, b-b..).

4.2.1 Numerical ‘LLFCmodel2007’

- a) All the ‘grains’ have the same ellipsoidal shape. They can be considered as single particles or included in fractal aggregates.
- b) Each particle is rotated to obtain the average light scattering values from an optically thin cloud of particles.
- c) The materials are astronomical silicate coated or not by an absorbing material (like carbon-black or darker). The two materials are defined by their complex refractive indices.
- d) The effective size of the particles is computed precisely. The size distribution follows that of Grün et al. 1985) for particles with sizes smaller than 10 μm (smaller 0.2 μm) and particles between 10 and 200 μm .

4.2.2 Experimental simulation

- a) Usually the grains and particles are irregular and of different sizes.
- b) Microgravity flights have been used to lift the cloud and avoid segregation by gravity. The real small particles and small aggregates stick together when lifted and make agglomerates which are the particles of the cloud. Their size distribution is measured on the screen of the instrument. The total mass in the vial is sufficiently small to allow having an optically thin cloud (the small number of particles is controlled on the screen of the instrument).
- c) Various materials which are supposed to compose cometary particles and asteroids (silicates, CC). The CC mass is mainly composed of carbon-black and amorphous coal. They allow to change the CC ratios in the different samples (mixtures).
- d) The effective size of the particles has to be estimated and adapted to have a similar size distribution than in LLFCmodel2007. Particles with smaller diameter than 10 μm cannot be measured. They are probably present in the mixtures; the smaller ones often stick on the largest particles. They have an influence on the scattered light. The aggregates have different porosities. If the constituent grain of an aggregate is larger than 5 μm , the particle is considered as a compact one.

As a function of the solar distance, the local polarization results with both simulations are very similar. Nevertheless, at 1.5 au, a difference is noticed. The polarization at 90° phase angle from LLFCmodel2007 calculated from the relation $P_{90^\circ}(\%) = (30 \pm 3) R^{0.5 \pm 0.1}$ is $(36.7 \pm 1.5) \%$ at 1.5 au (Fig. 7). The polarization obtained for mixture 2 $(36 \pm 2) \%$ is similar to this value. Mixture 3 with a polarization of $(29 \pm 2) \%$ seems to be closer to the local polarization as found in Fig. 6 (best fit for the phase curve). If the local polarization values are considered, a mixture intermediate between 2 and 3 would probably better fit the observations.

Note that none of the models can interpret the very important decrease in polarization at solar distances smaller than 0.5 au, which is probably due to changes in other parameters of the distribution of particles than their organics ratio (fragmentation of the particles, sublimation of various components, including minerals).

4.3 Influence of different physical parameters on the phase curves

The phase curves for the interplanetary dust particles are typical of irregular particles in clouds. As for cometary particles, the maximum in polarization decreases when the sub-micron size of the constituent grains in aggregates increases (mix 1 and mix 2). The maximum in polarization decreases progressively when the ratio of absorbing carbon over transparent materials decreases as the albedo increases (particles closer to the Sun), as suggested by the LLFCmodel2007. Following it, we have not considered other parameters such as the eventual decrease of the size of large, hundreds of micrometers, fluffy or compact particles (fragmentation during impacts or sublimation) and/or smaller ratio of aggregates of sub-micron sized grains (Hadamcik et al., 2009b) which can affect the polarization for solar distances smaller than about 0.4 au. The decrease of the average size of the absorbing carbon particles (compact or aggregates) from about 100 μm to 0.1 μm was previously studied with PROGRA2 (Hadamcik et al., 2009b, Fig. 10). The decrease in polarization is also noticed for transparent materials but the lower limit is about 10 μm ; for smaller sizes the polarization increases slightly. On the opposite, if the grain sub-micron size in the aggregates decreases (sublimation or thermal degradation), the polarization would increase (Hadamcik et al., 2009, Fig 9b). At solar distances smaller than 0.3 au, the fragmentation of the particles may be one reason of the observed drastic decrease of polarization but it is probably not sufficient. The destruction of the minerals must be also considered (Mann et al., 2004).

4.4. Presence and evolution of organics in the particles; effect on the polarization

The decrease in P_{max} from 1.5 to 0.5 au (Fig 7) can be linked to the increase of the local albedo (Levasseur-Regourd et al., 2001), which may be due to a decrease of absorbing materials when the solar distance decreases (Dumont and Levasseur-Regourd, 1988). Mann et al. (1994) and Mukai (1996) suggest a degradation of CC with decreasing heliocentric distance for solar distances smaller than 1.8 au. Silicates emission features in mid-infrared also increases when approaching the Sun, suggesting a decrease of the amorphous carbon (Reach et al., 2003). This is also coherent with the temperature variations calculated in LLFCmodel2007 between 1.5 au and 0.5 au from the Sun for particles with effective radius smaller than 2 μm . They found a temperature-distance factor of -0.33 for organics and -0.35 for amorphous carbon; it is very close to the -0.36 found for the local temperature retrieved from observations. The maximum temperature at 0.5 au, for organics or amorphous carbon compact particles of effective diameter of 1.5 μm would be 500-600 K and more than 850 K for fluffy fractal particles of organics with the same effective diameter and a size of the grains of 0.19 μm radius.

The thermal degradations of organics (or CC) are consistent with the degradation of cometary particles ejected by the nucleus when the temperature of the grains rises, in a first time when ejected in the coma, and later in the interplanetary medium when approaching the Sun. In fact, some gaseous species which were not directly ejected by the nucleus were speculated to originate from the destruction of materials present in the refractory components of the particles e.g. H_2CO , HCN , CO (Cottin and Fray, 2008). Some materials have been proposed as possible refractory organics in cometary particles, such as e.g. HCN polymers (Rettig et al., 1992); they begin to change at temperatures higher than 470 K, their products by thermal degradation seem to be mainly HCN and NH_3 (Fray et al., 2004). Tholins (polymeric hydrogenated carbon nitrides), which can be used as analogues of N-rich cometary organics,

are also thermally degraded at similar temperatures than HCN polymers with a mass loss up to 90 % of the initial mass and residues reorganized with a progressive increase of polyaromatic units (Bonnet et al., 2015; He et al., 2015). The N-rich aromatics are also found in Insoluble Organic Matter (IOM) in carbonaceous chondrites and have probably a cometary origin (Aleon et al., 2003). This material may also be the final residue of thermal degradation of poly-HCN or of tholins (Bonnet et al., 2015). When these components are thermal degraded, their carbon ratio increases in the residues and they become darker. But with the large mass loss the final albedo should not change a lot in the mixture with silicates. Carbon-black seems to be also thermal degraded in similar temperatures range i.e. between 740 K and 1000 K, the mass loss may be 40 % of the initial mass (Bredin et al., 2011).

With the Rosetta space mission experiments, numerous semi volatiles and refractory CC were found on the surface of 67P (Quirico et al., 2016) and in the ejected particles high molecular weight organics were also detected (Fray et al., 2016). The decrease of P_{\max} could probably be interpreted by the degradation of mixtures of refractory CC, for which degradation is possible at different temperatures depending on the grain particles size, their structure and their heliocentric distance.

Organics were found in IDPs and Mann et al. (1994) suggest a very important degradation of them mainly for fractal particles, for smaller distances than 100 solar-radii. The about 0 value of residual organics obtained by the simulation (LLFCmodel2007) at 0.5 au is a first approximation; it just presents the consistency of the observations with an important decrease of the organic ratio at the surface of the particles. This result may be restricted due e.g. to the unique refractive indices for the organics (laboratory measurements have shown that organics may be partially transparent depending of their composition and the fact that they darken when the temperature increases). The decrease of albedo may be due to the decrease of absorbing organics but a change of size distribution and a change of structure of the particles may also play a role.

4.5 Similar polarimetric phase curves and reliability of a sample

Phase curves similar to cometary ones may be obtained by other materials than carbonaceous ones and for different size distributions. Some mineral irregular particles can provide polarization phase curves close to cometary phase curves. In particular, Munoz & Hovenier, (2015) used a crushed Mg-rich olivine (forsterite) sample in sizes smaller than 20 μm and a sample with a size range smaller than 2 μm . Volten et al. (2006) estimated the refractive indices of the forsterite sample; they suggested imaginary values of 10^{-5} , i.e. a transparent sample and not a material of low-albedo. Their polarimetric phase curves are comparable to those of comets 1P/Halley and C/1975 N1 Kobayashi-Berger-Milon. For the very high polarization comet C/1995 O1 Hale-Bopp, in the same work, another sample, with aggregates of Mg-silicates with sub-micron-sized grains, seems to be a best analogue but as for the olivine (or forsterite), the material is transparent. The difference between these polarimetric phase curves is mainly the result of a difference in the grain size not of the materials. The spectral gradient in polarization of the olivine sample presents a positive spectral gradient as the majority of comets (Kolokolova et al., 2004). This kind of materials were found in cometary comae particles together with CC, as shown by remote or in-situ observations (see e.g. Wooden et al., 2017). Our past and present laboratory measurements with PROGRA2 (Hadamcik et al., 2007a; 2009b) have shown the importance of the presence of carbonaceous particles when trying to simulate cometary particles (with a global low-albedo). The precise numerical modelling of the irregular Sahara sand particles as possible cosmic dust, by Escobar et al. (2017), has shown the importance of irregularities on the surface for

polarization measurements, and can produce very excellent correlation with the experimental phase curves. Nevertheless, such modelling effort for mixtures of particles of different materials and structures seems to be out of reach for the time being. A polarimetric phase curve and other light scattering properties give indications on the properties of the object, but only if the used materials and sizes of the particles represent reliably the objects.

6. Conclusion

We try to simulate the light scattered by materials with composition and physical properties consistent with what is suspected for comets and for the interplanetary cloud. Cometary particles are made by mixtures of transparent and absorbing materials. We have demonstrated by experimental studies that the mixtures of silicates and organics into fluffy and compact particles following a constant power-law size distribution (coefficients -3.1 ± 0.5 for particles in the 10-100 μm range and -4.4 ± 0.6 for particles in the 100-200 μm) can reproduce the zodiacal light deduced local properties from observations. The parameters for the mixtures are consistent with the ones obtained previously from numerical simulations and consist of (35 ± 10) % in mass aggregates and (40 ± 5) % organics at 1.5 au decreasing to less than 0.1 % organics at 0.5 au. While, the composition of the interplanetary dust could be more complex, the present work identifies a reasonable set of parameters for the nature of the particles and their scattering properties. The presence of numerous organics, in very large particles and of sub-micron sized grains in aggregates either compact or with very high porosities, were proved by the Rosetta measurements. Such particles are ejected in the interplanetary medium and are suggested to constitute its major fraction, at least for solar distances below 1.5 au.

Acknowledgements

F. Pillier (LISE/CNRS/Sorbonne Univ.) is gratefully acknowledged for MEB analysis. We are grateful to the laboratories teams which provide us with their samples: N. Carrasco and G. Cernogora at LATMOS/IPSL with the PAMPRE experiment team for the tholins, H. Cottin and N. Fray from LISA/Université de Créteil for the HCN-polymers, N. Picot-Catel and L. Mannou from ENS/Paris for the enstatite and forsterite, A. Jambon from Institut des Sciences de la Terre de Paris for the basalt sample, J. Blum and R. Schraepler from Institut für Geophysik and Extraterrestrische Physik/Braunschweig for the random ballistic silica, J. Nuth and N. Johnson from Goddard Space Flight Center/NASA for the fluffy Mg&Fe-silicates, the Pennsylvania State University Coal Research Section for the lignite, A. Bush from Ecole Centrale/Paris for the heating of some samples. The parabolic flights, managed by Novespace, were funded by CNES and ESA. This work was partly supported by CNES and ESA in relation to observations of MIDAS on the Rosetta mission. We thank the two anonymous reviewers for their helpful questions and comments which considerably helped us to improve the paper.

References

- Agarwal J., Müller M., Reach W.T., et al., 2010. The dust trail of comet 67P/Churyumov-Gerasimenko between 2004 and 2006. *Icarus* 207, 992-1012.
- Aléon J., Robert F., Chaussidon M., Marty B., 2003. Nitrogen isotopic composition of macromolecular organic matter in interplanetary dust particles. *Geochim. Cosmochim. Acta*, 67, issue 19, 3773-3783.
- Bentley M.S., Schmied R., Mannel T., et al., 2016. Aggregate dust particles at comet 67P/Churyumov-Gerasimenko. *Nature* 537, 73-75.
- Bockelée-Morvan D., Rinaldi G., Erard S., et al., 2017. Comet 67P outbursts and quiescent coma at 1.3 au from the Sun; dust properties from Rosetta/VIRTIS-H observations. *MNRAS* 469, S443-S458.

- Bredin A., Larcher A.V., Mullins B., 2011. Thermogravimetric analysis of carbon black and engine soot - Towards a more robust oil analysis method. *Tribology International*, 44, 1642-1650.
- Brownlee D.E. 2016. Cosmic dust: building blocks of planets falling from the sky. *Elements*, 12, 165-170.
- Burns J.A., Lamy P.L., Soler S., 1979. Radiation forces on small particles in the solar system. *Icarus* 40, 1-48.
- Bus S.J. and Binzel R.P., 2002. Phase II of the small main-belt asteroid spectroscopic survey: A feature-based taxonomy. *Icarus* 158, 146-177.
- Cellino A., Gil-Hutton R., Belskaya I., 2015. Asteroids. In: *Polarimetry of stars and planetary systems*, L. Kolokolova, J. Hough, A.C. Levasseur-Regourd eds., Cambridge University Press, pp.360-375.
- Cottin H. and Fray N., 2008. Distributed sources in comets. *Space Sci. Rev.* 138, 179-197.
- Della Corte V., Rotundi A., Fulle M., et al., 2016. 67P/C-G inner coma dust properties from 2.2 au inbound to 2.0 outbound to the Sun. *MNRAS* 462, S210-S219.
- DeMeo F.E. and Binzel R.P., 2008. Comets in the near-Earth object population. *Icarus* 194, 436-449.
- DeMeo F.E., Binzel R.P., Slivan S.M., Bus S.J., 2009. An extension of the Bus asteroid taxonomy into the near-infrared. *Icarus* 202, 160-180.
- Dobrica E., Engrand C., Leroux et al., 2012. Transmission electron microscopy of CONCORDIA ultra-Carbonaceous Antarctic MicroMeteorites (UCAMMs): mineralogical properties. *Geochim. Cosmochim. Acta* 76, 68-82.
- Dumont R. and Sanchez F., 1975. Zodiacal light photopolarimetry. II. Gradients along the ecliptic and the phase functions of interplanetary matter. *A&A* 38, 405-412.
- Dumont R. and Levasseur-Regourd A.C., 1988. Properties of interplanetary dust from infrared and optical observations; I. Temperature, global volume intensity, albedo and their heliocentric gradients. *A&A*. 191, 154-160.
- Dumont R., Renard J.-B., Levasseur-Regourd A.C., Weinberg J.L., 1998. Disentangling the main populations of the zodiacal cloud from zodiacal light observations. *EPS* 50, 473-476.
- Engrand C. and Maurette M., 1998. Carbonaceous micrometeorites from Antarctica. *MPS* 33, 565-580.
- Escobar-Cerezo J., Palmer C., Munoz O., et al., 2017. Scattering properties of large irregular cosmic dust particles at visible wavelengths. *ApJ* 838: 74 (17p.).
- Fechtig H., Leinert C., Grün E., 1981. Interplanetary dust and zodiacal light. In: *Landolt-Börstein New Series VI/2A*, pp. 228-243.
- Flynn G.J., 1989. Atmospheric entry heating- A criterion to distinguish between asteroidal and cometary sources of interplanetary dust. *Icarus* 77, 287-310.
- Flynn G.J., 1994. Interplanetary dust particles collected from the stratosphere: physical, chemical, and mineralogical properties and implications for their sources. *PSS* 42, 1151-1161.
- Flynn G.J., Wirick S., Keller L.P., 2013. Organic grain coatings in primitive interplanetary dust particles: implications for grain sticking in the solar nebula. *EPS* 65, 1159-1166.
- Fray N., Bénilan Y., Cottin H., et al., 2004. Experimental study of the degradation of polymers: Application to the origin of extended sources in cometary atmospheres. *MPS* 39, Nr4, 581-587.
- Fray, N., Bardyn, A., Cottin, H., et al., 2016. High-molecular-weight organic matter in the particles of comet 67P/Churyumov-Gerasimenko. *Nature*, 538 (7623), 72.
- Fulle M. and Blum J., 2017. Fractal dust constrains the collisional history of comets. *MNRAS* 469, S39-S44.
- Fulle M., Marzani F., Della Corte V. et al., 2016. Evolution of the dust size distribution of comet 67P/Churyumov-Gerasimenko from 2.2 au to perihelion. *ApJ* 821, 19 (14 p.).
- Goidet-Devel B., Renard J.-B., Levasseur-Regourd A.C., 1995. Polarization of asteroids. Synthetic curves and characteristic parameters. *PSS* 43, 779-786.
- Greenberg J.M. and Hage J.I., 1990. From interstellar dust to comets- A unification of observational constraints. *ApJ* 361, 260-274.
- Grün E., Zook H.A., Fechtig H., Giese R.H., 1985. Collisional balance of the meteoritic complex. *Icarus* 62(2) 244-272.
- Grün E., Baguhl M., Svedhem H., Zook H.A., 2001. In situ measurements of cosmic dust. In: E. Grün, B.A.S. Gustafson, S.F. Dermott, H. Fechtig, eds, *Interplanetary dust*. Berlin: Springer-Verlag pp. 295-346.
- Grün E., Gustafson B.A.S., Dermott S., Fechtig H., eds, 2001. *Interplanetary dust*, A&A Library, Springer-Verlag, Berlin Heidelberg.
- Grün E., Horanyi M., Sternovsky Z., 2011. The lunar dust environment. *PSS* 59, 1672-1680.
- Hadamcik E. and Levasseur-Regourd A.C., 2003a. Imaging polarimetry of cometary dust: different comets and phase angles. *JQSRT* 79-80, 661-678.
- Hadamcik E. and Levasseur-Regourd A.C., 2003b. Dust evolution of comet C/1995 O1 (Hale-Bopp) by imaging polarimetric observations. *A&A* 403, 757-768.
- Hadamcik E., Renard J.-B., Levasseur-Regourd A.C., Lasue J., 2006. Light scattering by fluffy particles with the PROGRA2 experiment. *Mixtures of materials. JQSRT* 100, 143-156.
- Hadamcik E., Renard J.-B., Rietmeijer F.J.M., et al., 2007a. Light scattering by fluffy Mg-Fe-SiO and C mixtures as cometary analogs (PROGRA2 experiment). *Icarus* 190, 660-671.
- Hadamcik E., Renard J.-B., Lasue J., 2007b. Light scattering by low-density agglomerates of micron-sized grains with the PROGRA2 experiment. *JQSRT* 106, 74-89.

- Hadamcik E., Renard J.-B., Levasseur-Regourd A.C., Worms J.C., 2009a. Laboratory measurements of the light scattered by clouds of solid particles by imaging technique. In : *Light scattering Rev.* 4, A. Khokanovsky ed., Springer-Verlag, Berlin Heidelberg, pp. 31-70.
- Hadamcik E., Renard J.-B., Levasseur-Regourd A.C., et al., 2009b. Light scattering by agglomerates; Interconnecting size and absorption effects (PROGRA2 experiment). *JQSRT* 110, 1755-1770.
- Hadamcik E., Renard J.-B., Levasseur-Regourd A.C., Lasue J., 2011a. Laboratory measurements of light scattered by clouds and layers of solid particles using an imaging technique, In: *Proceedings of the NATO Advanced Study Institute on Special Detection Technique (Polarimetry) and Remote Sensing*, Yalta, Ukraine 20 September - 1 October 2010, NATO Science for Peace and Security Series C: Environmental Security, Mishchenko, M.I.; Yatskiv, Y.S.; Rosenbush, V.K.; Videen, G. (eds.), Springer, 137-176.
- Hadamcik E., Levasseur-Regourd A.C., Renard J.-B., et al., 2011b. Polarimetric observations and laboratory simulations of asteroidal surfaces: The case of 21 Lutetia. *JQSRT* 112, 1881-1890.
- Hadamcik E., Sen A.K., Levasseur-Regourd A.C., et al., 2013. Dust in comet 103P/Hartley 2 during EPOXI mission. *Icarus* 222, 774-785.
- Hadamcik E., Sen A.K., Levasseur-Regourd A.C., et al., 2014. Dust coma of comet C/2009 P1 (Garradd) by imaging polarimetry. *MPS* 49, 36-44.
- Hadamcik E. and Levasseur-Regourd A.C. 2016. Imaging polarimetry of comet 73P/Schwassmann-Wachmann 3 main fragments during its 2006 apparition. *PSS* 123, 51-62.
- Hadamcik E., Levasseur-Regourd A.C., Hines D.C., et al., 2017. Properties of dust particles in comets from photometric and polarimetric observations of 67P, *MNRAS* 462, S507-S515.
- Hanner M. 2003. The scattering properties of cometary dust. *JQSRT* 79-80, 695-705.
- Hanner M.S. and Bradley J.P. 2004. Composition and mineralogy of cometary dust. In: *Comets II*, M. Festou, H.U. Keller, H.A. Weaver, eds, Tucson: University of Arizona Press, pp. 555-564.
- Hörz F., Morrison D.A., Brownlee D.E., et al., 1975. Lunar microcraters- Implications for the micrometeoroid complex. *PSS* 23, 151-172.
- Hörz F., Bastien R., Borg J., et al., 2006. Impact features on Stardust: implications for comet 81P/Wild2 dust. *Science* 314, 1716-1719.
- He J., Buch A., Carrasco N., Szopa C., 2015. Thermal degradation of organics for pyrolysis in space : Titan's atmospheric aerosol case study. *Icarus* 248, 205-212.
- Ishiguro M., Watanabe J., Usui F., et al., 2002. First detection of an optical dust trail along the orbit of 22P/Kopff, *ApJ* 572, L117-L120.
- Ishiguro M., Kwon S.M., Sarugaku Y., et al., 2003. Discovery of the dust trail of the Stardust comet sample return mission target 81P/Wild 2. *ApJ* 589, L101-L104.
- Jewitt D., Weaver H., Agarwal J., et al., 2010. A recent disruption of the main-belt asteroid P/2010 A2. *Nature* 467, 817-819.
- Jewitt D., Agarwal J., Li J., Weaver H., et al., 2014. Disintegrating asteroid P/2013 R3. *ApJL* 784, L8.
- Jewitt D., Hsieh H., Agarwal J., 2015. The active asteroids. In: *Asteroids IV*, P. Michel, F.E. DeMeo, W.F. Bottke, eds, Univ. of Arizona Press, Tucson, pp. 221-241.
- Kawara K., Matsuoka Y., Sano K., et al., 2017. Ultraviolet to optical diffuse sky emission as seen by the Hubble Space Telescope Faint Object Spectrograph. *PASJ* 69, Issue 2, id 31.
- Keller L.P., Thomas K.L., McKay D.S., 1992. An interplanetary dust particle with links to CI chondrites. *Geochim. Cosmochim. Acta* 56, 1409-1412.
- Kim Y., Ishiguro M., Usui F., 2014. Physical properties of asteroids in comet-like orbits in infrared asteroid survey catalogs. *ApJ*, 789, 151 (9p.)
- Kiselev N., Rosenbush V., Levasseur-Regourd A.C., Kolokolova L., 2015. Polarimetry of comets. In: *Polarimetry of stars and planetary systems*, L. Kolokolova, J. Hough, A.C. Levasseur-Regourd, eds., Cambridge University Press, pp. 379-397.
- Kolokolova L., Kimura H., Kiselev N., Rosenbush V., 2007. Two different evolutionary types of comets proved by polarimetric and infrared properties of their dust. *A&A* 463, 1189-1196.
- Kolokolova L., Hanner M., Levasseur-Regourd A.C., Gustafson B.A.S., 2004. Physical properties of cometary dust from light scattering and emission. In: *Comets II*, M. Festou, H.U. Keller, H.A. Weaver, eds, Tucson: University of Arizona Press, 577-604.
- Kuroda D., Ishiguro M., Watanabe M., et al., 2017. Significantly high polarization degree if the very low-albedo asteroid (152679) 1998 KU2. *A&A* in press, arXiv:1712.01444v1.
- Langevin Y., Hilchenbach M., Ligier N., et al., and the COSIMA team, 2016. Typology of dust particles collected by the COSIMA mass spectrometer in the inner coma of 67P/Churyumov-Gerasimenko, *Icarus* 271, 76-97.
- Langevin Y., Hilchenbach M., Vincendou M., et al., and the COSIMA team, 2017. Optical properties of cometary particles collected by the COSIMA mass spectrometer on-board Rosetta during the rendezvous phase around comet 67P/Churyumov-Gerasimenko. *MNRAS* 469, S535-S549.
- Lasue J. and Levasseur-Regourd A.C., 2006. Porous irregular aggregates of submicron sized grains to reproduce cometary dust light scattering observations. *JQSRT* 100, 220-236.

- Lasue J., Lvasseur-Regourd A.C., Fray N., Cottin H., 2007. Inferring the interplanetary dust properties from remote observations and simulations. *A&A* 473, 641-649.
- Lasue J., Lvasseur-Regourd A.C., Hadamcik E., Alcouffe G., 2009. Cometary dust properties retrieved from polarization observations: Application to C/1995 O1 Hale-Bopp and 1P/Halley. *Icarus* 199, 129-144.
- Lasue J., Lvasseur-Regourd A.C., Lazarian A., 2015. Interplanetary dust, In: *Polarimetry of stars and planetary systems*. L. Kolokolova, J. Hough, A.C. Lvasseur-Regourd eds., Cambridge University Press, pp. 419-436.
- Leinert C., 1975. A measure of the interplanetary environment, *SSR* 18, 281-339.
- Leinert C. and Grün E., 1990. Interplanetary dust, In: *Physics and chemistry in Space – Space and Solar physics 30, Physics of the inner Heliosphere I*, R. Schwenn and E. Marsch eds, Springer-Verlag, Berlin Heidelberg.
- Leinert C., Bowyer S., Haikala L.K., et al., 1998. The 1997 reference of diffuse night sky brightness, *A&AS* 127, 1-99.
- Lvasseur-Regourd A.C., 1996. Optical and thermal properties of zodiacal dust, In: *Physics, Chemistry and Dynamics of Interplanetary dust*, B.A.S Gustafson & M.S. Hanner eds, ASP Conf. Series, Proceedings 150th colloquium of IAU, Gainesville, Florida, USA Aug. 1995, ASP 104, pp. 301-308.
- Lvasseur-Regourd A.C. and Hasegawa H. eds, 1991. *Origin and evolution of interplanetary dust*, Dordrecht-Boston, Kluwer Academic publisher.
- Lvasseur-Regourd A.C., Renard J.-B., Dumont R., 1991. Dust optical properties: A comparison between cometary and interplanetary grains. *ASR* 11, 175-182.
- Lvasseur-Regourd A.C., Cabane M., Haubourg V. 1999. Observational evidence for the scattering properties of interplanetary and cometary dust clouds: an update. *JQSRT* 63, 631-641.
- Lvasseur-Regourd A.C., Mann I., Dumont R., Hanner M.S., 2001. Optical and thermal properties of interplanetary dust. In: *Interplanetary dust*, E. Grün, B.A.S. Gustafson, S.F. Dermott, H. Fechtig eds, Berlin: Springer-Verlag, pp. 57-94.
- Lvasseur-Regourd A.C. and Hadamcik E., 2003. Light scattering by irregular dust particles in the solar system: observations and interpretation by laboratory measurements. *JQSRT* 79-80, 903-910.
- Lvasseur-Regourd A.C., Mukai T., Lasue J., Okada Y., 2007. Physical properties of cometary and interplanetary dust. *PSS* 55, 1010-1020.
- Lvasseur-Regourd A.C., Renard J.-B., Shkuratov Y., Hadamcik E., 2015. Laboratory studies. In: *Polarimetry of stars and planetary systems*, L. Kolokolova, J. Hough, A.C. Lvasseur-Regourd, eds., Cambridge University Press, pp. 62-80.
- Mann I, Okamoto H., Mukai T., Kimura H., Kutada Y., 1994. Fractal aggregate analogues for near solar analogues. *A&A* 291, 1011-1018.
- Mann I., Kimura H., Biesecker D.A., et al., 2004. Dust near the Sun. *SSR* 110, 269-305.
- Mann I., Czechowski A., Kimura H., et al., 2006. Physical properties of the dust in the Solar System and its interrelation with small bodies. In: *Asteroids, Comets, Meteors proceedings of the IAU 229 Symposium of IAU, Buzios, Rio de Janeiro, Brazil, Aug 7-12 2005*, L. Danielo, S. Ferraz, F. Angel, F. Julio eds, Cambridge University Press, pp. 41-65.
- Mannel T., Bentley M.S., Schmied R., et al., 2016. Fractal cometary dust- a window into early Solar system. *MNRAS* 462, S304-S311.
- Mukai T., 1996. Sublimation of Interplanetary dust, In: *Physics, Chemistry, and Dynamics of Interplanetary Dust*, B.A.S Gustafson and M.S. Hanner eds, ASP Conf. Series, Proceedings 150th colloquium of IAU, Gainesville, Florida, USA Aug. 1995, ASP 104, pp. 453-462.
- Mukai T., Nakamura A.M., Blum J., et al., 2001. Physical processes on interplanetary dust. In: *Interplanetary dust*, E. Grün, B.A.S. Gustafson, S.F. Dermott, H. Fechtig eds, Springer, Berlin, Heidelberg, pp. 445-507
- Nesvorny D., Jenniskens P., Levison H.F. et al., 2010. Cometary origin of the zodiacal cloud and carbonaceous micrometeorites: Implications for hot debris disks. *ApJ* 713, 816-836.
- Munoz O. and Hovenier J.W., 2015. Experimental scattering matrices of clouds of randomly oriented particles, In: *Polarimetry of stars and planetary systems*, L. Kolokolova, J. Hough, A.C. Lvasseur-Regourd eds, Cambridge University Press, pp. 130-138.
- Penttilä A., Lumme K., Hadamcik E., Lvasseur-Regourd A.C., 2005. Statistical analysis of asteroidal and cometary polarization phase curves. *A&A* 432, 1081-1090.
- Reach W.T., 1991. Zodiacal light II- Dust near ecliptic. *ApJ* 369, 529-543
- Reach W.T., Morris P., Boulanger F., Okumura K., 2003. The mid-infrared spectrum of the zodiacal and exozodiacal light. *Icarus* 164, 384-403.
- Reach W.T., Kelley M.S., Sykes M.V., 2007. A survey of debris trails from short period comets. *Icarus* 191, 298-322.
- Renard J.-B., Lvasseur-Regourd A.C., Dumont R., 1995. Properties of interplanetary dust from infrared and optical observations. II Brightness, polarization, temperature, albedo and their dependence on the elevation above the ecliptic. *A&A* 304, 602-608.
- Renard J.-B., Hadamcik E., Lvasseur-Regourd A.C., 1996. Polarimetric CCD imaging of comet 47P/Ashbrook-Jackson and variability of polarization in the inner coma of comets. *A&A* 316, 263-269.

- Renard J.-B., Worms J.C., Lemaire T., et al., 2002. Light scattering by dust particles in microgravity: polarization and brightness imaging with the new version of the PROGRA2 instrument. *Appl. Opt.* 41, 609-618.
- Rotundi A., Sierks H., Della Corte V., et al., 2015. Dust measurements in the coma of comet 67P/Churyumov-Gerasimenko inbound to the Sun. *Science* 347, issue 6220, aaa3905.
- Rowan-Robinson M. and May B., 2013. An improved model for the infrared emission from the zodiacal dust cloud: cometary, asteroidal and interstellar dust. *MNRAS* 429, 2894-2902.
- Quirico, E., Moroz, L.V., Schmitt, B., et al., 2016. Refractory and semi-volatile organics at the surface of comet 67P/Churyumov-Gerasimenko: Insights from the VIRTIS/Rosetta imaging spectrometer. *Icarus*, 272, 32-47.
- Schulz R., Hilchenbach M., Langevin Y., et al., 2015. Comet 67P/Churyumov-Gerasimenko sheds dust coat accumulated over the past four years. *Nature* 518, issue 7538, 216-218.
- Sykes M.V. and Walker R.G., 1992. Cometary dust trails. I-Survey. *Icarus* 95, 180-210.
- Sykes M.V., Grün E., Reach W.T., Jenniskens P., 2004. The Interplanetary dust complex and comets, In: Comets II, M.C. Festou, H.U. Keller, H.A. Weaver eds, Univ Arizona Press, Tucson, 745, pp. 677-693.
- Tholen D.J., 1989. Asteroid taxonomic classifications, In: Asteroids II; Proceedings of the conference, Tucson, AZ, Univ. of Arizona Press 1139-1150.
- Thomas K.L., Blanford G.E., Clemmett S.J., et al., 1995. An asteroidal breccia: The anatomy of a cluster IDP. *Geochim. Cosmochim. Acta* 59, 2797-2815.
- Vernazza P., Delbo M., King P.L., et al., 2012. High surface porosity as the origin of emissivity features in asteroid spectra, *Icarus* 221, 1162-1172.
- Vernazza P., Marsset M., Beck P., et al., 2015. Interplanetary dust particles as samples of icy asteroids. *ApJ* 806, 204 (10P).
- Volten H., Munoz O., Brucato J.R., Hovenier J.W., et al., 2006. Scattering matrices and reflectance spectra of forsterite particles with different size distributions. *JQSRT* 100, 429-436.
- Wooden D.H., Ishii H.A., Zolensky M.E., 2017. Cometary dust: the diversity of primitive refractory grains. *Phil. Trans. R. Soc. A375*: 20160260.
- Worms J.C., Renard J.-B., Hadamcik E., Levasseur-Regourd A.C., 1999. Results of the PROGRA2 experiment: An experimental study in microgravity of scattered polarized light by dust particles with large size distribution. *Icarus* 142, 281-297.
- Zolensky M.E., Zega T.J., Yano H., et al., 2006. Mineralogy and petrology of comet 81P/Wild 2 nucleus samples, *Science* 314, 1735-1739.

Highlights

- Confirmation of observational polarization results by an experimental approach
- Analogues of inner interplanetary dust at different solar distances
- Confirmation of the decrease of organics ratio closer to the Sun
- Aggregated particles with power law size distributions between 10 μ m and 200 μ m
- Particles structure and sizes compatible with Rosetta's findings on comet 67P